

Aggressive Visual Perching with Quadrotors on Inclined Surfaces

Jeffrey Mao¹, Guanrui Li¹, Stephen Nogar², Christopher Kroninger², and Giuseppe Loianno¹

Abstract—Autonomous Micro Aerial Vehicles (MAVs) have the potential to be employed for surveillance and monitoring tasks. By perching and staring on one or multiple locations aerial robots can save energy while concurrently increasing their overall mission time without actively flying. In this paper, we address the estimation, planning, and control problems for autonomous perching on inclined surfaces with small quadrotors using visual and inertial sensing. We focus on planning and executing of dynamically feasible trajectories to navigate and perch to a desired target location with on board sensing and computation. Our planner also supports certain classes of nonlinear global constraints by leveraging an efficient algorithm that we have mathematically verified. The on board cameras and IMU are concurrently used for state estimation and to infer the relative robot/target localization. The proposed solution runs in real-time on board a limited computational unit. Experimental results validate the proposed approach by tackling aggressive perching maneuvers with flight envelopes that include large excursions from the hover position on inclined surfaces up to 90° , angular rates up to 600 deg/s , and accelerations up to 10 m/s^2 .

I. INTRODUCTION

Micro Aerial Vehicles (MAVs) have great speed and maneuverability however they tend to have very low flight time. Current solutions limit battery life to around 10-20 minutes. Fortunately for many missions such as environmental monitoring, it is unnecessary to remain in hover for the whole mission duration. In general, by perching and staring on one or multiple location, a MAV can greatly extend its mission time saving power without the need to frequently replace batteries. This motivates the need of autonomous perching solutions to conserve energy and extend the mission time.

In this paper, we tackle the autonomous perching problem on inclined surfaces with quadrotors solely using on board cameras and Inertial Measurement Unit (IMU) as shown in Fig. 1. Inclined flat surfaces like walls and rooftops are plentiful especially in urban environments and by focusing on this avenue, we can aim to greatly reduce the energy consumption of multiple types of mission. The proposed autonomous perching problem is challenging for several reasons. The maneuver, to intercept the target, requires large excursions from the hover position. In addition, the vehicle must generate and execute dynamically feasible trajectories respecting the actuator and sensor constraints despite the



Fig. 1: Aggressive visual perching sequence maneuver for a 90° inclined surface.

presence of nonholonomic and underactuation constraints. Finally, in our case, the maneuver has to be accomplished relying exclusively on on board minimalist sensor data (camera and IMU) and limited computational unit. The ability to execute these challenging maneuvers can be leveraged as well in several other scenarios including reaction to sudden changes in the operational conditions for obstacle avoidance or navigation in constrained environments.

This paper presents multiple contributions. First, we show how to generate and execute dynamically and physically feasible trajectories for perching on inclined surfaces. Our planning solution efficiently supports certain classes of nonlinear constraints such as maximum thrust limit through the use of an efficient bound checking algorithm that we have mathematically verified. The planner versatility to incorporate a diverse set of constraints makes it potentially able to support different perching or adhesion mechanisms. Second, our approach relies solely on on board sensing and computation for navigation and to infer the relative robot/target configuration. Finally, this is the first time that a fully autonomous quadrotor system is able to perch on any flat inclined surface with minimum mechanical modifications. Other works either assume the availability of a motion capture system [1] or require the landing point to be in the field of view at the starting location based on visual servoing approaches [2], [3].

This paper is organized as follows. Section II details the relevant works in the perching area using aerial vehicles. Section III presents an overview of the key algorithms and hardware modules employed in our approach. Section IV details our approach to achieving autonomous perching purely through on-board sensing and computation. Section V validates our approach considering several autonomous perching maneuvers on inclined surfaces that include flight envelopes with large excursions from the hover position. Finally, Section VI contains our concluding remarks on the subject.

II. RELATED WORKS

Prior works on perching with quadrotors on inclined surfaces focus on solving the trajectory generation and/or

¹The authors are with the New York University, Tandon School of Engineering, Brooklyn, NY 11201, USA email: {jm7752, lguanrui, loiannog}@nyu.edu.

²The authors are with the U.S. Army Research Laboratory, 2800 Powder Mill Road, Adelphi, MD 20783, USA. email: {stephen.m.nogar, christopher.m.kroninger}.civ@mail.mil.

This work was supported by the ARL grant DCIST CRA W911NF-17-2-0181 and the young researchers program "Rita Levi di Montalcini" 2017 grant PGR17W9W4N.

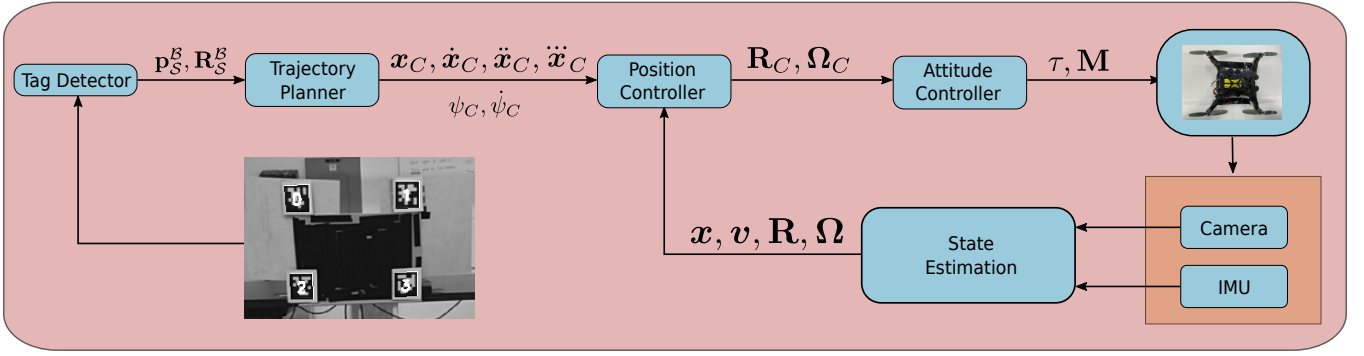


Fig. 2: System architecture for the perching task

control problems [4], [1] relying exclusively on motion capture systems. These solutions do not address the design challenges and requirements when deploying robots equipped with embedded on board sensors and computationally limited units. Furthermore, the approach presented in [4] relies on composition of multiple control modes with linearized controllers without guaranteeing feasibility of the maneuver. Other works focus on the perching mechanism design. The approach proposed in [5] considers specific cylindrical objects and the proposed solution restricts the range of possible perch locations due to the size of the gripper and specific shape of the object. Other solutions rely on dry adhesives [6], [7], [8] or suction gripper solutions [9], [10] mechanisms or active perching mechanisms solutions [9]. However, the use of active perching mechanism solutions further increases the vehicle's payload and energy requirements, while concurrently decreasing the overall flight time. Finally, in [11] a bio-inspired trajectory planning approach is presented. However, the work relies on an actuated gripper for specific cylindrical objects and relies on expensive 3D cameras to locate perching locations. Finally, visual servoing approaches [2], [3] have recently shown some autonomous perching results without the use of motions capture but are highly dependent on objects' shapes and require the object to initially be in the field of view.

Other works employ fixed wing solutions and focus on perching mechanism designs [12], [13]. Fixed wing solutions have lower maneuverability with respect to quadrotor solutions. Moreover, these have the ability to hover in place and navigate in confined and can generate both slow and fast, agile movements, making them a very versatile solution to solve different tasks. The flight time is obviously more restricted with respect to fixed wing solutions and this further motivates for this class of aerial vehicles the usefulness to provide autonomous perching solutions.

Compared to the aforementioned solutions, we concurrently guarantee dynamical and physical feasibility of the planned trajectories. Furthermore, our approach relies exclusively on on board sensor and estimation and small computational unit. In the presented case, we focus on the ability to guarantee on board autonomous perching with dynamically and physically feasible trajectories. We leverage the differential flatness property and develop an efficient planning

algorithm to generate trajectories for a quadrotor without the limitation to first order systems [14] or composition of multiple control modes relying on linearized controllers [4]. The proposed approach is agnostic with respect to the type of active/passive perching mechanism, due to the ability to support a diverse set of constraints which could conform to different attachment/adhesion mechanisms.

III. SYSTEM OVERVIEW

The proposed system architecture is shown in Fig. 2 is a quadrotor running with a Qualcomm[®] Snapdragon[™] board and 4 brushless motors. The Qualcomm[®] Snapdragon[™] has a Qualcomm[®] Hexagon[™] DSP, Wi-Fi, Bluetooth, GPS, one core processor along with a downward and front-facing camera with a 160 degree field of view along with an IMU. For perching, we employ VELCRO[®] material mounted in the ventral part of the vehicle.

The software framework has been developed in ROS¹ on a Linux kernel and includes a state estimation algorithm running at 500 Hz composed of a Unscented Kalman Filter (UKF) and Visual Inertial Odometry (VIO) [15] which processes images at 30 Hz as well as a target detection algorithm. The downward facing camera is solely devoted to state estimation of the quadrotor and the front-facing camera is used to detect the perch target's position and orientation. Furthermore, the system runs on board a position and attitude controllers plus a trajectory planner to generate and execute the feasible planned path to the target. The approaches are presented in detail in the next Section.

IV. APPROACH

Let the inertial frame \mathcal{I} be represented by the following three axes $[\mathbf{e}_1 \ \mathbf{e}_2 \ \mathbf{e}_3]$. The quadrotor body frame \mathcal{B} is represented by $[\mathbf{b}_1 \ \mathbf{b}_2 \ \mathbf{b}_3]$. This frame origin is located at the center of mass of the vehicle. Consequently, we denote the relative position of the quadrotor with respect to the \mathcal{I} frame as $\mathbf{x} = [x \ y \ z]^T$ and the relative orientation as $\mathbf{R} = [\mathbf{b}_1 \ \mathbf{b}_2 \ \mathbf{b}_3] \in SO(3)$. The perching target frame is denoted with \mathcal{S} and is represented by the axes $[\mathbf{s}_1 \ \mathbf{s}_2 \ \mathbf{s}_3]$. The relevant frames and configuration settings are depicted in Fig. 3. The perching problem from time $t = t_0$ to $t = t_f$ with $t \in \{t_0, \dots, t_i, \dots, t_f\}$ requires the vehicles to navigate by

¹www.ros.org

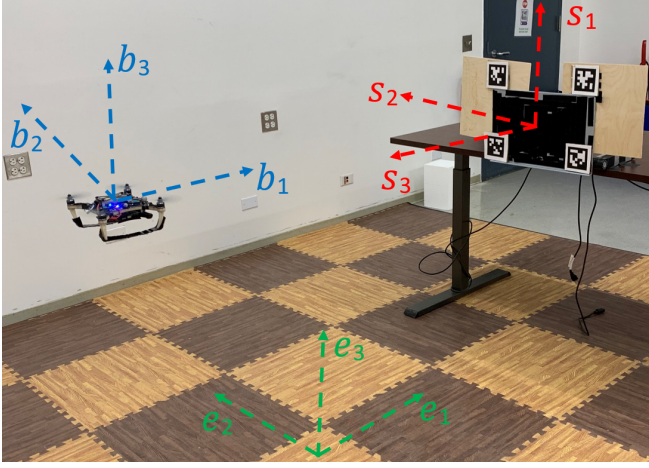


Fig. 3: Setup overview and frame convention definitions.

planning and executing a feasible trajectory (i.e., generating a sequence of $\mathbf{R}(t) \in SO(3)$ and $\mathbf{x}(t) \in \mathbb{R}^3$) such that $\mathcal{B} \equiv \mathcal{S}$ at $t = t_f$. The problem is decomposed in several steps. First, the vehicle visually locates the target and estimates the relative configurations from the \mathcal{B} to \mathcal{S} frames (i.e., relative position $\mathbf{p}_S^B \in \mathbb{R}^3$ and orientation $\mathbf{R}_S^B \in SO(3)$). Second, the relative configuration information is incorporated at the planning and control levels to generate and execute trajectories that are dynamically and physically feasible.

In the following Section IV-A we briefly review the vehicle's system dynamics and control. Section IV-B describes the proposed perception pipeline including autonomous navigation and target localization. Section IV-C details our trajectory planning approach and how we leverage in this context the system dynamics and the relative configuration constraint to guarantee the correct plan and execution.

A. Modeling and Control

The system dynamic model in the inertial frame \mathcal{I} is

$$\begin{aligned} \dot{\mathbf{x}} &= \mathbf{v}, \dot{\mathbf{v}} = \mathbf{a}, m\mathbf{a} = \mathbf{R}\tau\mathbf{e}_3 - m\mathbf{g}\mathbf{e}_3, \\ \dot{\mathbf{R}} &= \mathbf{R}\hat{\Omega}, \mathbf{J}\dot{\Omega} + \Omega \times \mathbf{J}\Omega = \mathbf{M}, \end{aligned} \quad (1)$$

where $\mathbf{x}, \mathbf{v}, \mathbf{a} \in \mathbb{R}^3$ are the position, velocity, acceleration of the quadrotor's center of mass in Cartesian coordinates with respect to the inertial frame \mathcal{I} , \mathbf{R} represents the orientation of the quadrotor with respect to \mathcal{I} , $\Omega \in \mathbb{R}^3$ is the angular velocity of the quadrotor with respect to \mathcal{B} , $m \in \mathbb{R}$ denotes the mass of the quadrotor, $\mathbf{J} \in \mathbb{R}^{3 \times 3}$ represents its inertial matrix with respect to \mathcal{B} , $g = 9.81 \text{ m/s}^2$ is the standard gravitational acceleration, $\mathbf{M} \in \mathbb{R}^3$ is the total moment with respect to \mathcal{B} , $\tau \in \mathbb{R}$ represents the total thrust to the quadrotor, and the $\hat{\cdot}$ represents the mapping such that $\hat{\mathbf{a}}\mathbf{b} = \mathbf{a} \times \mathbf{b}, \forall \mathbf{a}, \mathbf{b} \in \mathbb{R}^3$.

To achieve aggressive maneuvers, we apply a nonlinear geometric controller that was leveraged in our previous work [16] to achieve agile flight in indoor environments. First, $\mathbf{k}_R, \mathbf{k}_\Omega, \mathbf{k}_x, \mathbf{k}_v \in \mathbb{R}^{3 \times 3}$ are positive definite diagonal matrix representing the feedback gains for the errors in orientation, angular velocity, position and velocity respectively.

Based on those feedbacks, the control inputs are thrust τ and moment \mathbf{M} selected as

$$\begin{aligned} \tau &= (-\mathbf{k}_x\mathbf{e}_x - \mathbf{k}_v\mathbf{e}_v + m\mathbf{g}\mathbf{e}_3 + m\ddot{\mathbf{x}}) \cdot \mathbf{R}\mathbf{e}_3 = \mathbf{f} \cdot \mathbf{R}\mathbf{e}_3, \\ \mathbf{M} &= -\mathbf{k}_R\mathbf{e}_R - \mathbf{k}_\Omega\mathbf{e}_\Omega + \Omega \times \mathbf{J}\Omega \\ &\quad - \mathbf{J}(\hat{\Omega}\mathbf{R}^\top\mathbf{R}_C\Omega_C - \mathbf{R}^\top\mathbf{R}_C\dot{\Omega}_C). \end{aligned} \quad (2)$$

$\mathbf{e}_R, \mathbf{e}_\Omega, \mathbf{e}_x, \mathbf{e}_v \in \mathbb{R}^3$ are the orientation, angular velocity, position and velocity errors this is detailed in works [17], [18], and the \cdot_C are the command or desired values obtained from the planning algorithm or computed using the differential flat outputs of the quadrotor system.

B. State Estimation and Perching Surface Localization

For quadrotor autonomous navigation, we leverage our previous work [15], where we showed aggressive maneuvers combining visual and inertial data via VIO and UKF.

The perching localization method is unimportant for our system as long as it gives both position and pose. For our use experiments perching localization is achieved through the use of four Apriltags [19] placed on the corners of the targets. By placing these Apriltags on the four corner, we can easily calculate the exact center of the landing pad by averaging these position while also leaving a large portion of VELCRO[®] to land on. Our software perception pipeline polls images from the front camera and runs an Apriltag localization algorithm. In our system, we use ids 0, 1, 2, 3 of the Apriltag family 36h11 to characterize the corners. The quadrotor continues to poll the front-facing camera to recognizes all 4 Apriltags Ids, and takes the first sample image as the target configuration location \mathbf{p}_S^B and orientation \mathbf{R}_S^B with respect to the robot frame. To reduce sensitivity to the noise detection process, we average the tags' position and quaternions to obtain the target center position and orientation in the camera frame.

C. Planning for Aggressive Perching

After acquiring the target location and orientation to satisfy the end goal of reaching the target and perching, we plan a differentially smooth and dynamically feasible trajectory by exploiting the differential flatness property of the quadrotor. This allows us to shift the planning problem defined at the beginning of this Section to the flat space of the vehicle $\{\mathbf{x}, \psi\} = \{x, y, z, \psi\}$. ψ is the yaw angle. We employ a set of polynomial splines P_d to represent the quadrotor trajectory:

$$\begin{aligned} P_d(t) &= \begin{cases} p_{1d}(t) & \text{if } t \in [t_0, t_1] \\ \vdots & \\ p_{id}(t) & \text{if } t \in [t_{i-1}, t_i] \\ \vdots & \\ p_{fd}(t) & \text{if } t \in [t_{f-1}, t_f] \end{cases}, \\ p_{id}(t) &= \sum_{n=0}^N c_{nid}t^n, \end{aligned} \quad (3)$$

where $d \in \{1, 2, 3, 4\}$ corresponds to the dimension of the flat space of the quadrotor system composed by the flat outputs $\{x, y, z, \psi\}$, p_{id} represents the i^{th} polynomial making up the full trajectory of P_d , $c_{nid} \in \mathbb{R}$ is the n^{th} coefficient of p_{id} , and N represents the polynomial order chosen for each spline. We chose polynomial splines to represent to the trajectory because polynomials are smooth and described completely through its coefficients $c_{nid}, i = 1, \dots, f$ and $n = 0, \dots, N$, which can help accelerate the computation if the polynomial order N is selected appropriately.

In the following, we formulate this trajectory planning problem as a Quadratic Programming (QP) optimization based on polynomial splines. The trajectory optimization will also need to satisfy perching, actuators, and sensing constraints globally in a time efficient manner. We first declare a cost function as the squared norm of the j^{th} order derivative summed in all dimensions

$$\sum_{d=1}^4 \int_{t_0}^{t_f} \left\| \frac{d^j P_d(t)}{dt^j} \right\|^2 dt. \quad (4)$$

In previous works [15], [20], the formulation of snap was shown to be closely related to minimizing the angular rate's derivative, and minimizing the jerk was related to the angular velocity. Our planner supports both formulations of this cost. We also see in eq. (4) that for each dimension in the cost is independent, so they can be optimized separately. As a result, we will refactor eq. (4) as a square matrix multiplied by two vectors for a single dimension. First, we formulate the case for one polynomial spline in the form $\mathbf{c}_{id}^T \mathbf{Q}_i \mathbf{c}_{id}$ as

$$\min_{\mathbf{c}_{id}} \mathbf{c}_{id}^T \left(\int_{t_{i-1}}^{t_i} \frac{d^j \mathbf{t}}{dt^j} \frac{d^j \mathbf{t}^T}{dt^j} dt \right) \mathbf{c}_{id} \quad (5)$$

where $\mathbf{t} \in \mathbb{R}^N$ represents a vector of time defined as $[1, t, t^2, \dots, t^N]^T$ and $\mathbf{c}_{id} \in \mathbb{R}^N$ is the vector that consists of all the coefficients of p_{id} . $\mathbf{Q}_i \in \mathbb{R}^{N \times N}$ is the cost matrix formed from the center integral in eq. (5). It should be noted that \mathbf{Q}_i is identical for all dimensions, d , so it has no subscript d . We can then convert eq. (5) into one unified cost for dimension d in the form $\mathbf{c}_d^T \mathbf{Q} \mathbf{c}_d$ by stacking the matrices diagonally $\text{Diag}(\mathbf{Q}_1, \dots, \mathbf{Q}_i, \dots, \mathbf{Q}_f) = \mathbf{Q}$ and forming $\mathbf{c}_d \in \mathbb{R}^{Nf}$ as a vector of all the \mathbf{c}_{id} stacked vertically. We can then formulate an equality constraint in the form $\mathbf{b}_{id} = \mathbf{A}_{id} \mathbf{c}_{id}$. The term \mathbf{b}_{id} is a vector consisting of all the user defined constraints for dimension d that are imposed at t_i . \mathbf{A}_{id} is defined by transposing \mathbf{t} into a row vector then stacking \mathbf{t} and its derivatives up to order 4 vertically,

$$\begin{bmatrix} p_{id}(t_i) \\ \dot{p}_{id}(t_i) \\ \vdots \end{bmatrix} = [\mathbf{t}(t_i) \quad \dot{\mathbf{t}}(t_i) \quad \dots]^T * \mathbf{c}_{id}. \quad (6)$$

The constraints on higher order terms like velocity and accelerations are optional to declare in eq. (6). We can simply stack matrices in eq. (6) diagonally, $\text{Diag}(\mathbf{A}_{1d}, \dots, \mathbf{A}_{id}, \dots, \mathbf{A}_{fd})$, to create the combined constraint for all trajectories in a dimension. Additionally, a

continuity constraint between the endpoints of all splines is enforced for derivative orders up to the fourth order to ensure smoothness. The first order derivative case is

$$\begin{bmatrix} 0 \\ 0 \\ \vdots \\ 0 \end{bmatrix} = \begin{bmatrix} \dot{\mathbf{t}}(t_1) & -\dot{\mathbf{t}}(t_1) & 0 & \dots \\ 0 & \dot{\mathbf{t}}(t_2) & -\dot{\mathbf{t}}(t_2) & \dots \\ \vdots & \ddots & \ddots & \vdots \\ 0 & \dots & \dot{\mathbf{t}}(t_{f-1}) & -\dot{\mathbf{t}}(t_{f-1}) \end{bmatrix} \begin{bmatrix} \mathbf{c}_{1d} \\ \mathbf{c}_{2d} \\ \vdots \\ \mathbf{c}_{fd} \end{bmatrix}. \quad (7)$$

Eq. (7) constraint is replicated to the fourth order and combined with eq. (6) constraints by stacking the matrices vertically creating a unified equality constraint matrix \mathbf{A}_d .

We can add additional inequality constraints formatted the same as eq. (6) \mathbf{A}_{id} for each spline and combine them in the same way to get \mathbf{G}_d . We can then formulate the combined constraint and costs in to 4 separate QP optimization problems to be solved in parallel for each dimension such to speed up the overall solution time. For each QP dimension the optimization problem is detailed below

$$\begin{aligned} \min_{\mathbf{c}_d} \quad & \mathbf{c}_d^T \mathbf{Q} \mathbf{c}_d \\ \text{s.t.} \quad & \mathbf{A}_d \mathbf{c}_d = \mathbf{b}_d \\ & \mathbf{y}_d \leq \mathbf{G}_d \mathbf{c}_d \leq \mathbf{z}_d \end{aligned} \quad (8)$$

where the inequality constraint are between a lower bound \mathbf{y}_d and upper bound \mathbf{z}_d respectively. In case the QP dimensions are not separable due to joint constraints across dimensions the same structure is achieved by stacking for each dimension its \mathbf{A}_d diagonally and stacking four copies of \mathbf{Q} diagonally. Each of the vectors, \mathbf{c}_d , \mathbf{z}_d , \mathbf{y}_d , and \mathbf{b}_d , are in turned stacked vertically for each dimension. In the following section, we will discuss the perception, state and actuator constraints specific to executing perching tasks.

1) *Perching Perception and Physical Constraints:* Inspired by [15], we exploit the differential flatness property of our model to derive a relationship between the vehicle's center of mass acceleration, $\ddot{\mathbf{x}}$ and rotation matrix \mathbf{R} . First we look at the dynamical model established in eq. (1). We can derive that the nominal thrust as

$$\tau = m \|\ddot{\mathbf{x}} + g\mathbf{e}_3\|. \quad (9)$$

Based on the nonholonomic property of a quadrotor system, the generated force is along the \mathbf{b}_3 axis of the body frame of a quadrotor; therefore, the \mathbf{b}_3 should satisfy

$$\mathbf{b}_3 = \frac{\ddot{\mathbf{x}} + g\mathbf{e}_3}{\|\ddot{\mathbf{x}} + g\mathbf{e}_3\|}. \quad (10)$$

Using eq. (10), we can define \mathbf{b}_3 at the end of the perching at t_f through an acceleration constraint as

$$\ddot{\mathbf{x}}(t_f) = \alpha \mathbf{s}_3 - g\mathbf{e}_3, \quad (11)$$

where $\alpha = \|\ddot{\mathbf{x}}(t_f) + g\mathbf{e}_3\| \in \mathbb{R}$ corresponds to the pre-defined acceleration of the quadrotor selected by the user. The planned $\ddot{\mathbf{x}}$ is then injected in the thrust in eq. (2). The \mathbf{s}_3 direction on the inclined surfaces is extracted from the last column of the matrix \mathbf{R}_S . This orientation \mathbf{R}_S is obtained combining the outcome of the state estimation algorithm with

the target detector, which also provides \mathbf{p}_S . These quantities allow us to fully define the target configuration with respect to the inertial frame and provide the constraints required to accomplish the perching maneuver. To enforce this maneuver at control level, the rotation matrix, we impose that in eq. 2, \mathbf{R}_C should be chosen according to

$$\mathbf{R}_C = [\mathbf{b}_{1,C} \quad \mathbf{b}_{2,C} \quad \mathbf{b}_{3,C}] \quad (12)$$

where

$$\mathbf{b}_{1,C} = \frac{\mathbf{b}_{2,des} \times \mathbf{b}_3}{\|\mathbf{b}_{2,des} \times \mathbf{b}_3\|}, \quad \mathbf{b}_{2,C} = \mathbf{b}_3 \times \mathbf{b}_1, \\ \mathbf{b}_{2,des} = [-\sin \psi_{des}, \quad \cos \psi_{des}, \quad 0]^\top, \quad \mathbf{b}_{3,C} = \frac{\mathbf{f}}{\|\mathbf{f}\|}.$$

The desired yaw angle ψ_{des} can be chosen by the user. Generally, we select it such that $\mathbf{b}_{2,des}$ is parallel to \mathbf{s}_2 , which can be known from \mathbf{R}_S . This reveals the relationship between quadrotor's acceleration and the \mathbf{R}_C , which is useful since our approach plans trajectories in the flat space of the quadrotor, and our planned goal is $\mathbf{R}_C \approx \mathbf{R}(t_f) \equiv \mathcal{S}$. The commanded angular rate is then

$$\dot{\Omega}_C = \mathbf{R}_C^\top \dot{\mathbf{R}}_C. \quad (13)$$

Next, additional constraints have to be placed on the impact velocity to ensure that the quadrotor is neither moving too quickly such that it bounces off the target nor too slowly risking that it does not properly adhere to the target. We take this aspect into account by imposing additional velocity constraints in the target proximity

$$v_{min} \leq \dot{\mathbf{x}}(t_f) \cdot \mathbf{s}_3 \leq v_{max}, \quad (14)$$

where v_{min} is the minimum impact velocity and v_{max} is the maximum. These values are dependent on the perching mechanism. Finally, the vehicle must complete most of its rotation before its impact with the surface rather than try to pivot at the target. This is to avoid the rim of the vehicle impacting the target surface by taking into account the vehicle's physical extension. Should the vehicle begin rotating too late in its trajectory, the front end will collide with the landing pad before reaching the desired attitude. This aspect is expressed by enforcing an additional acceleration range by a given $q\%$ tolerance in proximity of the target. In order to apply the inequality constraint to our optimization, we discretize the equation as

$$(1 - q)(\alpha \mathbf{s}_3 - g \mathbf{e}_3) \leq \ddot{\mathbf{x}}(t) \leq (1 + q)(\alpha \mathbf{s}_3 - g \mathbf{e}_3), \\ \forall t \in \{t_f - t_k + j * dt\} \quad j \in \mathbb{Z} \ \& \ 0 \leq j < \frac{t_k}{dt}, \quad (15)$$

where dt is the sampling time of our trajectory planner and t_k is the time prior to the impact which is user defined.

2) *Actuators Constraints*: The planning algorithm also considers the limits of the actuators. If we refer to eq. (9), then it follows that there are lower and upper bounds τ_{min} and τ_{max} respectively that the vehicle's thrust τ should respect. We can then incorporate the actuator constraint formulated as

$$\tau_{min}^2 \leq \|m\ddot{\mathbf{x}} + mg\mathbf{e}_3\|_2^2 \leq \tau_{max}^2. \quad (16)$$

Algorithm 1 GLOBAL BOUND CHECKING (GBC)

Returns true if $H(t) < b \ \forall t \in [t_0, t_f]$. $H(t)$ is any polynomial. $b \in \mathbb{R}$ is an upper bound

```

1: Let  $F(t) = H(t) - b$ ;
2: if  $F(t_0) > 0$  or  $F(t_f) > 0$  then
3:   return FALSE
4: end if
5: if STURM( $F(t), t_0, t_f$ )  $> 0$  then
6:   return FALSE
7: end if
8: return TRUE

```

This constraint is nonlinear, therefore, cannot be formulated in the QP optimization. We will describe how our system satisfies this condition in the next section.

3) *Optimization Procedure*: For our planner, we use the QP to solve the constraints described in eqs. (11), (14), and (15). Next, we use Algorithm 1 to verify if the constraint described in eq. (16) is met. We do not apply Algorithm 1 to the inequality constraints in eqs. (14) and (15) because they are linear constraints and can be efficiently resolved within the QP optimization. Should the global bounds be violated, we increase the trajectories' time iteratively and recursively to solve the QP until eq. (16) is met. Because the lower order derivatives are correlated with the higher order derivatives, as we increase the time, the lower order terms are minimized. We visualize this process in Fig. 4 whereby increasing the allotted time for a minimum snap trajectory, the constraint from eq. (16) is met through iteratively expanding the time and checking the bounds.

Inspired by [21], Algorithm 1 checks if given any polynomial, $H(t)$, then is $H(t) < b \ \forall t \in [t_0, t_f]$ true. For our algorithm, $H(t)$ is set to the squared norm of the thrust described in eq. (16). We apply the constraint on the squared norm of the thrust in eq. (16) instead of the norm because the square root of a polynomial is unlikely to be a polynomial. Algorithm 1 works by leveraging the function STURM [22] which returns the number of roots of any arbitrary polynomial, $H(t)$ in a bound $t \in [t_0, t_f]$. A proof of algorithm 1 is included in the appendix along with a more detailed description of STURM's implementation. Using algorithm 1, we can ensure that our generated trajectory does not violate eq. (16) without checking each point of our trajectory. This time reduction is quantified in Table. I.

4) *Computation Reduction via Sparsity*: The equality constraint in eqs. (6) and (7) can be reformulated to increase their sparsity by shifting the time of each segments as follows

$$P_d(t) = \begin{cases} p_{1d}(t - t_0) & \text{if } t \in [t_0, t_1] \\ \vdots & \\ p_{id}(t - t_{i-1}) & \text{if } t \in [t_{i-1}, t_i] \\ \vdots & \\ p_{fd}(t - t_{f-1}) & \text{if } t \in [t_{f-1}, t_f]. \end{cases} \quad (17)$$

The time shifted spline refactors the constraints matrices

in eqs. (6) and (7) reducing the number of non-zeros in our equality constraint by approximately one half. The sparsity increases because each segment effectively starts at $t = 0$. Since $\mathbf{t}(0)$, defined in eq. (6), and all its derivatives have only one nonzero term when evaluated at 0, time shifting effectively halves the number of non-zeros in our constraint matrix. This increases the sparsity of our matrices and contributes to speeding up the overall optimization process which provides extremely high rate planning solutions.

V. EXPERIMENTAL RESULTS

The experiments are conducted in the new indoor testbed with a flying space of $10 \times 5 \times 4 \text{ m}^3$ at the ARPL lab at New York University. The ground truth data is collected using a Vicon² motion capture system at 100 Hz. Navigation is performed solely based on the on board VIO system running at 500 Hz. Our landing pad is mounted on an adjustable desk that allows us to control height. Also, the adhesive is attached to an adjustable stand which allows us to control the surface angle along a specific axis. We selected a tolerance, $q = 0.1$, sampling time, $dt = 0.01 \text{ s}$, time before impact, $t_k = 0.15 \text{ s}$ and $\alpha = 3.3 \text{ m/s}^2$ as the hyperparameters of eqs. (11) and (15). Finally, we set the impact velocity bound of eq. (14) as the minimum impact velocity, $v_{min} = 0.4 \text{ m/s}$, and maximum impact velocity, $v_{max} = 0.6 \text{ m/s}$.

First, we evaluate the computational time and scalability of our trajectory generator by analyzing the time taken to resolve a complete trajectory generation problem given 3 and 10 randomly selected waypoints respectively. In particular, we also verify that our optimization procedure respects the maximum thrust bound in addition to the aforementioned linear inequality constraints. We choose to minimize the snap norm in the cost. This trajectory times spanned an initial $t_0 = 0 \text{ s}$ and end $t_f = 1 \text{ s}$. We then applied a bound on the maximum thrust, $\tau_{max} = 4.5 \text{ N}$. We observe that the thrust shrinks for each iteration in Fig. 4 as time increases. This process repeats till our condition is respected, where $t_f = 1.4 \text{ s}$. Computational results are reported in Table I. To ensure consistency of our results, we obtained the results by re-running the optimizer 5 times and averaging the outcome. We leverage the C++ OOQP library [23] to solve our QP formulation. Our framework is also able to perform sequential quadratic programming to solve some classes of nonlinear optimization problems leveraging the NLOPT [24] library at the cost of speed. For the following experiment, we compared whether using a nonlinear optimizer to ensure the thrust is respected, or using our current formulation of checking after the QP was faster. The following experiments all use a polynomial order $N = 14$. We then compare the computation speed of using a nonlinear optimizer to enforce the global thrust bound at every time point versus our current procedure. This procedure consists of solving without the nonlinear thrust bound, using Algorithm 1 to check if this is respected, and adding time to violating segments till the global bounds are respected. We provide results for this

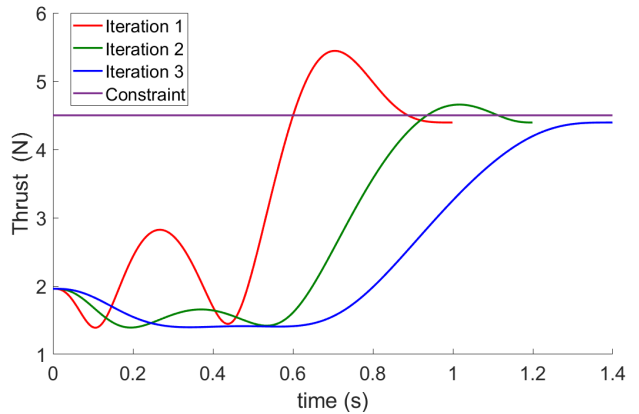


Fig. 4: Iterations through the GBC reducing thrust for perching trajectory.

specific scenario in Table I. The nonlinear optimization takes on the order of a $100\times$ longer to solve than performing a QP algorithm and checking afterwards. This indicates that checking that our current approach of doing multiple QP optimizations is better than trying to solve a single more complex nonlinear optimization.

We then proceed to evaluate our approach for perching on an inclined surface as shown in Fig. 1 considering two challenging inclination angles of 60° and 90° . These trajectories were created using a polynomial of order 14 and by minimizing the jerk's norm. In Fig. 5, we present the trajectory planning, control tracking, and localization results for the most challenging perching maneuver at 90° . We do not report the results on y-axis is excluded from Fig. 5 because the motion along that axis has not significant variations during the perching task. We also plot the current thrust vector in Fig. 5 (right) to further show that the constraint during perching is correctly enforced during the execution of the maneuver. As demonstrated, our additional constraints imposed through the eqs. (11) and (15) enforce the rotation to complete slightly before reaching the target. To further show that the proposed maneuver is particularly aggressive and challenging, we present the angular rates achieved during 90° perching on the three Cartesian axes in Fig 6. Our vehicle achieves angular rates close 600 deg/s , which to the best of our knowledge have never been achieved in the past for such a small scale vehicle using on board computation and visual perception for both state estimation and target localization.

Finally to validate the consistency, performance, and robustness of our algorithm, we use 2 different surface inclinations at two target distances of 1.7 m and 3 m respectively. We consider target locations up to 3 m since

Optimizer	Num. Waypoints	Computation Time (ms)
QP+GBC	3	4
	10	18
NLOPT	3	527
	10	1253

TABLE I: Computation time of our approach as a function of the number of waypoints.

²www.vicon.com

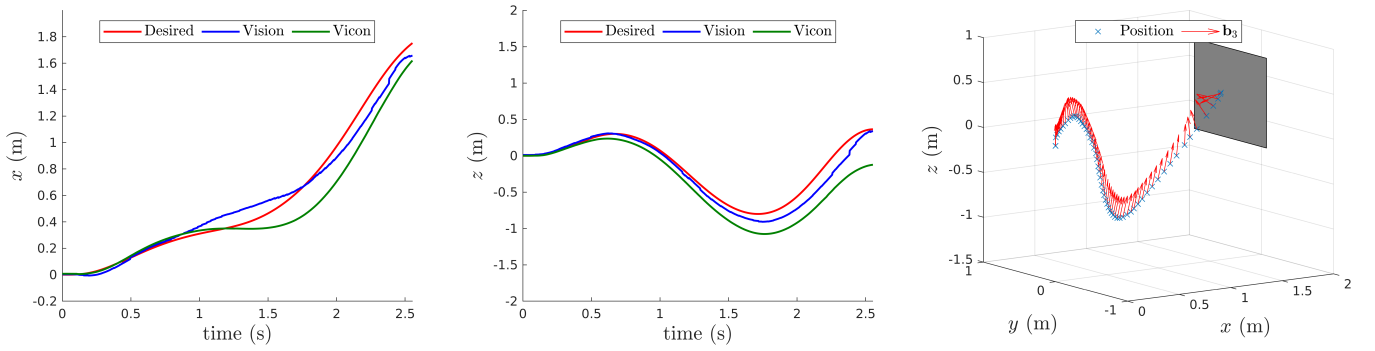


Fig. 5: Trajectory tracking and localization results for 90° surface inclination from a distance of 1.7 m. The blue crosses represent the quadrotor position, whereas the arrows represent the thrust vector.

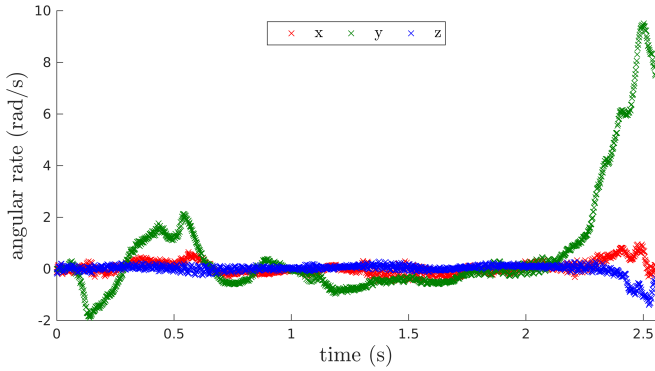


Fig. 6: Angular rate during a 90° perching maneuver.

for our setup, this has been verified to be the maximum distance to reliably detect the Apriltags. Table II shows the relevant trajectory tracking and state estimation RMSE metrics of these experiments. Furthermore, we repeat the procedure 5 times for each distance and surface inclinations and record the successful perching rate as seen in Table III. A successful perching is defined as the quadrotor adhering to the target and remaining attached. The lower success rate at 60° is due to the Apriltag accuracy falling for a worse viewing angle and further target. We observe that the tracking error is mostly located toward the end of the trajectory as depicted in Fig. 5 since once the vehicle is rotating prior to impact the perching location, it is very difficult to control its position. However, we still see our controller succeeding in the perch in these conditions. Overall, we see that our approach is able to generate reliable perching maneuver based on on board perception with cm level accuracy both in term of localization and control tracking of the maneuver.

Component		1.7 m		3 m	
		Tracking	Estimation	Tracking	Estimation
60°	x (m)	0.0500	0.0145	0.0378	0.0401
	y (m)	0.0325	0.0851	0.0732	0.0714
	z (m)	0.1509	0.0714	0.1321	0.0452
90°	x (m)	0.0503	0.0314	0.0948	0.0660
	y (m)	0.0539	0.0533	0.0360	0.0045
	z (m)	0.1081	0.0405	0.0911	0.0485

TABLE II: Tracking and Estimation RMSE for different surface inclinations and distances.

Furthermore, these success rates and tracking errors are agnostic with respect to the tested starting positions as well as surface inclination.

Target Distance (m)	Surface Angle	Success rate
1.7	60°	4/5
	90°	4/5
3	60°	3/5
	90°	4/5

TABLE III: Success rate statistics as a function of the inclined surface and the target distance.

VI. CONCLUSION

In this paper, we presented the planning, control, and perception methodologies to achieve autonomous visual perching with small quadrotors relying exclusively on on board computation and sensing. Our results show that we are able to generate aggressive and challenging perching maneuvers up to 90° inclined surfaces, angular rates up to 600 deg/s, and accelerations up to 10 m/s^2 . These results show the agility and robustness of our real-time autonomous perching.

Future works will focus on two research directions. First, we aim to leverage consecutive target detection across the entire planned maneuver to have a receding-horizon planning strategy. Continuous target information introduces the possibility to refine the trajectory in real-time to compensate for possible drifts or unmodelled effects during flight and consequently increases the resilience and precision for target interception. In this context, it is interesting to study the trade-off among the dynamic feasibility, aggressive behavior of the perching maneuver, and maximizing the visibility of the target. Second, we will work on enforcing the planning objectives and constraints at the control level by formulating a nonlinear MPC control problem where the sensors and actuator constraints can be embedded as additional terms in the optimization cost function or as constraints.

APPENDIX

A. Sturm's Theorem

Sturm's theorem [22] states that the number of roots for a polynomial, $H(t)$ in an interval $[t_0, t_f]$ is equal to the

difference in sign changes of the Sturm's sequence between $S(t_0)$ and $S(t_f)$ is defined in the equation below

$$S(t) = \begin{cases} S_0(t) = H(t) \\ S_1(t) = \dot{H}(t) \\ S_{i+1}(t) = -\text{Rem}(S_{i-1}, S_i) \\ \vdots \\ S_N(t) = -\text{Rem}(S_{N-2}, S_{N-1}) \in \mathbb{R} \end{cases}, \quad (18)$$

where the $\text{Rem}(S_{i-1}, S_i)$ returns the algebraic remainder of $\frac{S_{i-1}}{S_i}$. To evaluate the number of roots between $t \in [0, 2]$ for $H(t) = t^4 + t^3 - t - 1$. First calculate the Sturm sequence,

$$S(t) = \begin{cases} S_0(t) = t^4 + t^3 - t - 1 \\ S_1(t) = 4t^3 + 3t^2 - 1 \\ S_2(t) = 0.1875t^2 + 0.75t + 0.9375 \\ S_3(t) = -32t - 64 \\ S_4(t) = -0.1875 \end{cases} \quad (19)$$

We evaluate this sequence's signs at $t = 0$ as $[-, -, +, -, -]$. This sequence has 2 sign changes. Next, we calculate the sequence at $t = 2$ as $[+, +, +, -, -]$. There is 1 sign change. Subtracting the number of sign changes at $t = 0$ from $t = 1$, we find 1 root for $H(t)$ in the domain $[0, 2]$.

B. Proof of Algorithm 1

First, we leverage the intermediate value theorem. The intermediate value theorem state that given a continuous function $H(t)$ whose domain contains the values $[t_0, t_f]$ then $\forall i \in [H(t_0), H(t_f)]$ there must exist a corresponding $t_i \in [t_0, t_f]$ such that $i = H(t_i)$. Since our trajectory is continuous, this theorem holds in our case. Now let's prove that our algorithm works by contradiction. Assume, there exists a $t_i \in [t_0, t_1]$ such that $H(t_i) > b$ where b is the global bound, and all conditions of Algorithm 1, $H(t_0) < b$, $H(t_f) < b$, and $H(t_i) - b \neq 0 \forall t_i \in [t_0, t_f]$ are true.

If this is the case, then we can apply the intermediate value theorem and construct a domain $[t_0, t_i]$ and a range $[H(t_0), H(t_i)]$. We know that $H(t_0) < b$ and $H(t_i) > b$, then $b \in [H(t_0), H(t_i)]$. Therefore, based on the intermediate value theorem, there must exist a $t_j \in [t_0, t_i]$ such that $H(t_j) = b$. However, we see $H(t_j) = b$ is a contradiction with respect to the condition $H(t_j) - b \neq 0 \forall t_j \in [t_0, t_f]$. As $[t_0, t_i] \subset [t_0, t_f]$ by construction, this condition also holds true for all $t_j \in [t_0, t_i]$. Since, this is a contradiction there can exist no such number $t_i \in [t_0, t_1]$ such that $H(t_i) > b$ if our algorithm returns true.

REFERENCES

- [1] J. Thomas, M. Pope, G. Loianno, E. Hawkes, M. Estrada, H. Jiang, M. Cutkosky, and V. Kumar, "Aggressive flight for perching on inclined surfaces," *Journal of Mechanisms and Robotics*, vol. 8, 12 2015.
- [2] J. Thomas, G. Loianno, K. Daniilidis, and V. Kumar, "Visual servoing of quadrotors for perching by hanging from cylindrical objects," *IEEE Robotics and Automation Letters*, vol. 1, no. 1, pp. 57–64, 2016.
- [3] H. Zhang, B. Cheng, and J. Zhao, "Optimal trajectory generation for time-to-contact based aerial robotic perching," *Bioinspiration & Biomimetics*, vol. 14, 10 2018.
- [4] D. Mellinger, N. Michael, and V. Kumar, "Trajectory generation and control for precise aggressive maneuvers with quadrotors," *The International Journal of Robotics Research*, vol. 31, no. 5, pp. 664–674, 2012.
- [5] W. Chi, K. H. Low, K. H. Hoon, and J. Tang, "An optimized perching mechanism for autonomous perching with a quadrotor," in *IEEE International Conference on Robotics and Automation (ICRA)*, 2014, pp. 3109–3115.
- [6] A. Kalantari, K. Mahajan, D. Ruffatto, and M. Spenko, "Autonomous perching and take-off on vertical walls for a quadrotor micro air vehicle," in *IEEE International Conference on Robotics and Automation (ICRA)*, 2015, pp. 4669–4674.
- [7] E. W. Hawkes, D. L. Christensen, E. V. Eason, M. A. Estrada, M. Heverly, E. Hilgemann, H. Jiang, M. T. Pope, A. Parness, and M. R. Cutkosky, "Dynamic surface grasping with directional adhesion," in *IEEE/RSJ International Conference on Intelligent Robots and Systems*, 2013, pp. 5487–5493.
- [8] L. Daler, A. Klaptocz, A. Briod, M. Sitti, and D. Floreano, "A perching mechanism for flying robots using a fibre-based adhesive," in *IEEE International Conference on Robotics and Automation*, 2013, pp. 4433–4438.
- [9] H. Tsukagoshi, M. Watanabe, T. Hamada, D. Ashli, and R. Iizuka, "Aerial manipulator with perching and door-opening capability," in *2015 IEEE International Conference on Robotics and Automation (ICRA)*, 2015, pp. 4663–4668.
- [10] C. C. Kessens, J. Thomas, J. P. Desai, and V. Kumar, "Versatile aerial grasping using self-sealing suction," in *IEEE International Conference on Robotics and Automation (ICRA)*, 2016, pp. 3249–3254.
- [11] K. M. Pope, M. S. Johannes, K. C. Wolfe, R. A. Hegeman, J. M. Hatch, J. L. Moore, K. D. Katyal, B. Y. Yeh, and R. J. Bamberger, "Autonomous grasping robotic aerial system for perching (agrasp)," in *2018 IEEE/RSJ International Conference on Intelligent Robots and Systems (IROS)*, 2018, pp. 1–9.
- [12] J. Moore, R. Cory, and R. Tedrake, "Robust post-stall perching with a simple fixed-wing glider using LQR-trees," *Bioinspiration & Biomimetics*, vol. 9, no. 2, May 2014.
- [13] A. L. Desbiens, A. T. Asbeck, and M. R. Cutkosky, "Landing, perching and taking off from vertical surfaces," *The International Journal of Robotics Research*, vol. 30, no. 3, pp. 355–370, 2011.
- [14] Z. Zhang, P. Xie, and O. Ma, "Bio-inspired trajectory generation for uav perching," in *IEEE/ASME International Conference on Advanced Intelligent Mechatronics*, 2013, pp. 997–1002.
- [15] G. Loianno, C. Brunner, G. McGrath, and V. Kumar, "Estimation, control, and planning for aggressive flight with a small quadrotor with a single camera and imu," *IEEE Robotics and Automation Letters*, vol. PP, pp. 1–1, 11 2016.
- [16] G. Loianno, C. Brunner, G. McGrath, and V. Kumar, "Estimation, control, and planning for aggressive flight with a small quadrotor with a single camera and imu," *IEEE Robotics and Automation Letters*, vol. 2, no. 2, pp. 404–411, April 2017.
- [17] T. Lee, M. Leok, and N. H. McClamroch, "Nonlinear Robust Tracking Control of a Quadrotor UAV on SE(3)," *Asian Journal of Control*, vol. 15, no. 2, pp. 391–408, 2013.
- [18] G. Loianno, Y. Mulgaonkar, C. Brunner, D. Ahuja, A. Ramanandan, M. Chari, S. Diaz, and V. Kumar, "Smartphones power flying robots," in *IEEE/RSJ International Conference on Intelligent Robots and Systems*, Hamburg, Germany, Sept 2015, pp. 1256–1263.
- [19] E. Olson, "AprilTag: A robust and flexible visual fiducial system," in *Proceedings of the IEEE International Conference on Robotics and Automation (ICRA)*. IEEE, May 2011, pp. 3400–3407.
- [20] G. Loianno, Y. Mulgaonkar, C. Brunner, D. Ahuja, A. Ramanandan, M. Chari, S. Diaz, and V. Kumar, "A swarm of flying smartphones," in *2016 IEEE/RSJ International Conference on Intelligent Robots and Systems*, 10 2016, pp. 1681–1688.
- [21] Z. Wang, X. Zhou, C. Xu, J. Chu, and F. Gao, "Alternating minimization based trajectory generation for quadrotor aggressive flight," 2020.
- [22] P. Sturm, *Collected Works of Charles François Sturm*. Springer; 2009th edition, 01 2009, vol. 6, pp. 345–390.
- [23] E. M. Gertz and S. J. Wright, "Object-oriented software for quadratic programming," *ACM Trans. Math. Softw.*, vol. 29, no. 1, p. 58–81, Mar. 2003. [Online]. Available: <https://doi.org/10.1145/641876.641880>
- [24] S. G. Johnson, "The nlopt nonlinear-optimization package," <https://github.com/stevengj/nlopt>, 2007.